

Cluster induced quenching of galaxies in the massive cluster XMMXCS J2215.9-1738 at $z \sim 1.5$ traced by enhanced metallicities inside half R_{200}

C. Maier¹, M. Hayashi², B. L. Ziegler¹, and T. Kodama³

¹ University of Vienna, Department of Astrophysics, Tuerkenschanzstrasse 17, 1180 Vienna, Austria
e-mail: christian.maier@univie.ac.at

² National Astronomical Observatory of Japan, Osawa, Mitaka, Tokyo 181-8588, Japan

³ Astronomical Institute, Tohoku University, Aramaki, Aoba-ku, Sendai 980-8578, Japan

Received ; accepted

ABSTRACT

Aims. Cluster environments at $z < 0.5$ were found to increase the gas metallicities of galaxies which enter inner regions of the clusters where the density of the intracluster medium is high enough to remove their hot halo gas by ram-pressure stripping effects and to stop the inflow of pristine gas. To extend these studies to $z > 1$, the most massive clusters known at these redshifts are the sites where these environmental effects should be more pronounced and more easily observed with present day telescopes.

Methods. We explore the massive cluster XMMXCS J2215.9-1738 at $z \sim 1.5$ with KMOS spectroscopy of $H\alpha$ and $[NII] \lambda 6584$ covering a region that corresponds to about one virial radius. Using published spectroscopic redshifts of 108 galaxies in and around the cluster we computed the location of galaxies in the projected velocity vs. position phase-space to separate our cluster sample into a virialized region of objects accreted longer ago (roughly inside half R_{200}) and a region of infalling galaxies. We measured oxygen abundances for ten cluster galaxies with detected $[NII] \lambda 6584$ lines in the individual galaxy spectra and compared the mass-metallicity relation of the galaxies inside half R_{200} with the infalling galaxies and a field sample at similar redshifts.

Results. We find that the oxygen abundances of individual $z \sim 1.5$ star-forming cluster galaxies inside half R_{200} are comparable, at the respective stellar mass, to the higher local SDSS metallicity values. The metallicities of these galaxies in the inner part of the cluster are higher by 0.1–0.2 dex, at a given mass, than the metallicities of infalling galaxies and of field galaxies at $z \sim 1.5$. This effect is more pronounced when using the O3N2 metallicity calibration compared to the N2 calibration, which can be explained by the different locations of cluster and field galaxies in the $[OIII] \lambda 5007/H\beta$ vs. $[NII] \lambda 6584/H\alpha$ diagram involving two line ratios compared to one line ratio information in the case of the N2 relation. The enhanced metallicities of cluster galaxies at $z \sim 1.5$ inside $0.5R_{200}$ indicate that the density of the intracluster medium in this massive cluster becomes high enough toward the cluster center such that the ram pressure exceeds the restoring pressure of the hot gas reservoir of cluster galaxies and can remove this gas reservoir initiating quenching, although the galaxies continue to form stars, at slightly lower rates, using the available cold gas in the disk which is not stripped.

Key words. Galaxies: evolution – Galaxies: clusters: general – Galaxies: star formation – Galaxies: abundances

1. Introduction

While local and low-redshift clusters host large fractions of passive galaxies, with increasing redshift the star-forming (SF) population becomes larger. Since clusters of galaxies grow by accreting mass from their surroundings, the SF galaxies observed in high- z clusters must be the progenitors of the local passive galaxies. The $1 < z < 2$ redshift range hosts the emergence of the Hubble sequence of disks and elliptical galaxies and the buildup of a significant fraction of the stellar mass in the universe (e.g., Dickinson et al. 2003; Drory et al. 2005), being a transition epoch for clusters. At higher redshifts, forming clusters (protoclusters) consisting of mostly SF galaxies are forming a vast majority of their stellar content (e.g., Chiang et al. 2017). At later epochs ($z < 1$) many massive clusters virialize and most galaxies in their central parts are passive. Thus, this $1 < z < 2$ transition period when cluster galaxies are at the onset of environmental influences is a crucial time to investigate their properties and the mechanisms driving their evolution.

While studies of the mass-metallicity relation (MZR), chemical evolution and physical conditions of the interstellar medium (ISM) of SF *field* galaxies at these redshifts are now based on larger samples (e.g., Zahid et al. 2014; Kashino et al. 2017), the samples of *cluster* SF galaxies at $z > 1$ with studied metallicities are still very small. There is an ongoing debate about environmental signatures in the chemical enrichment of cluster galaxies, especially at $z > 1$. The few available samples are small (compared to field samples), affected by selection biases and the metallicity calibrator used, and produced some contradictory results. Kulas et al. (2013) found a 0.15 dex metallicity enhancement for $z \sim 2.3$ proto-cluster galaxies with respect to field counterparts at lower masses (by stacking galaxies with non-detected $[NII]$ emission lines), but no difference at higher masses. Shimakawa et al. (2015) found higher metallicities in proto-cluster members at $z > 2$ than in the field for $10 < \log(M/M_\odot) < 11$, by measuring metallicities based on $[NII]/H\alpha$ from stacked spectra. On the other hand, Valentino et al. (2015) found lower $[NII]/H\alpha$ ratios in $z \sim 2$ protocluster galaxies than in the field. Kacprzak et al. (2015) and Tran et al. (2015) used

stacked [NII]/H α ratios (including upper limits for [NII]) and found a similar MZR relation for field and cluster galaxies at $z \sim 2.1$ and $z \sim 1.62$, respectively.

Most of these studies of the MZR of cluster galaxies at $z > 1$ used the [NII] $\lambda 6584$ /H α ratio to determine metallicities with the N2-calibration (Pettini & Pagel 2004). The [NII]/H α ratio involves two emission lines (ELs) close in wavelength to each other and has some benefits: it can be observed at the same time also with higher resolution spectroscopy, the ratio is quite insensitive to extinction correction, and, from the ground, H α and [NII] $\lambda 6584$ can be followed all the way to redshift $z \sim 2.5$ (the limit of the near-infrared K-band). On the other hand, one main issue with the [NII]/H α ratio is that the [NII] $\lambda 6584$ line is often too weak to be detected in individual spectra at higher redshifts, therefore the stacking of spectra of several cluster galaxies was often used in the literature to study their chemical enrichment. Another problem is that the contamination of [NII] by night-sky lines can produce spurious metallicities relying only on [NII]/H α . This issue was investigated by Magdis et al. (2016), who used K-band Multi Object Spectrograph (KMOS) observations of KROSS (KMOS Redshift One Spectroscopic Survey) galaxies at $z \sim 1$. They found that imperfect subtraction of OH sky-lines affected 113 galaxies with no [NII] detection in their sample with distances $< 7\text{''}$ between the expected central λ of [NII] $\lambda 6584$ and sky-lines, producing wrong [NII] upper limits flux measurements and spurious metallicities from stacked spectra. They concluded that very weak [NII] $\lambda 6584$ lines partly overlapping with strong sky-lines may not be used to determine reliable metallicities based on using [NII]/H α only. In the samples of cluster galaxies at $z > 1.6$ with MZR studies mentioned above, it is possible that there are galaxies with no detection of [NII] and a likely problematic measurement of the [NII] $\lambda 6584$ EL flux (from stacking these spectra) due to the OH sky-lines residuals at the position of [NII], which could bias the resulting metallicity measurement from stacked spectra.

At lower redshifts, using a sample of SF cluster galaxies at $z \sim 0.2$ and $z \sim 0.4$, Maier et al. (2016, 2019) found higher metallicities, at a given mass, for cluster galaxies in the inner parts of seven massive LoCuSS clusters and one CLASH cluster. Maier et al. (2016, 2019) compared their observational findings with metallicity-SFR-mass bathtub model predictions with inflowing gas (Lilly et al. 2013) and deduced a slow-quenching (strangulation) scenario in which the gas metallicities can increase after removal of the hot halo gas reservoir because the interstellar medium (ISM) is no longer diluted by the inflow of pristine gas. During strangulation the inflow of new gas is cut out, but the cold ISM disk is not directly perturbed. In this case the star formation can continue, using the gas available in the disk (resulting in higher gas-phase metallicities) until the cold gas is completely used up.

These observational studies were compared with high-resolution cosmological hydrodynamic simulations of Bahé et al. (2013), who computed the density of the intracluster medium (ICM) and derived the ram pressure in clusters. The conclusion was that the ICM becomes dense enough at $R \sim R_{200}$, in $z < 0.5$ massive clusters with $M_{200} \sim 10^{15} M_{\odot}$, to remove the *hot* halo gas surrounding massive galaxies ($10 < \log(M/M_{\odot}) < 11$) by ram-pressure stripping (RPS) effects. For lower mass galaxies ($9 < \log(M/M_{\odot}) < 10$), the ICM becomes dense enough to remove their *hot* halo gas already further out at $R \sim 2R_{200}$. Maier et al. (2019) further deduced that, while slowly quenching for 1-2 Gyrs, galaxies travel to denser inner regions of the cluster where the RPS exceeds also the restoring pressure of the cold gas, eventually completely quenching

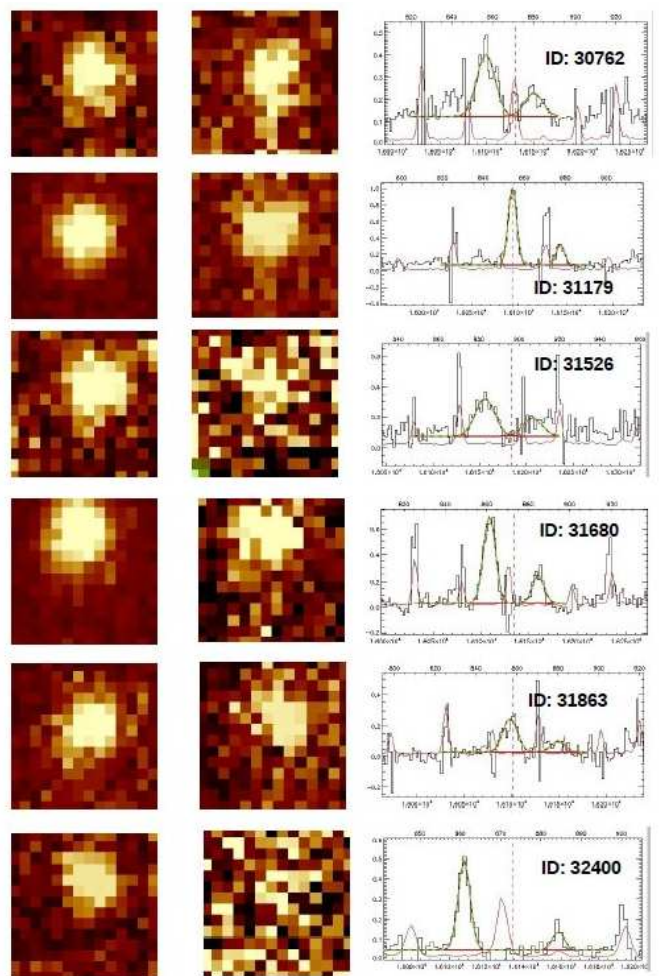


Fig. 1. The six galaxies of the main *SFvirialized* sample. Shown in each row, from left to right: ionized gas map as observed in H α with KMOS, ionized gas map as observed in [NII] $\lambda 6584$ with KMOS, extracted spectrum (black solid line) over an area of 25 spaxels with the fitted Gaussians by KUBEVIZ to H α and [NII] $\lambda 6584$ shown in green and the noise spectrum as a red solid line. The panels on the right show that the measurements of H α and [NII] $\lambda 6584$ are not affected by strong sky-lines (peaks of the red solid lines).

star formation by stripping the *cold* gas in a *rapid* phase. This *slow-then-rapid* quenching scenario is also in agreement with the theoretical study of Steinhauser et al. (2016), who used ram-pressure stripping simulations employing the moving-mesh code AREPO (Springel 2010) to follow at high resolution the interaction of a galaxy cluster with infalling galaxies. Steinhauser et al. (2016) found that, typically, their model galaxies continue to form stars with only slightly modified rates as a result of the stripping of the hot gaseous halos (strangulation) of the galaxies. On the other hand, the cold gas of their simulated galaxies is stripped only during pericenter passages with small pericenter distances leading to a full quenching of star formation on a short timescale.

As discussed also in Maier et al. (2019), there is a significant difference between this *slow-then-rapid* scenario and the “delayed-then-rapid” scenario of Wetzel et al. (2013). In the “slow” quenching phase the galaxies are already affected by the environment because strangulation was initiated, while in the “delayed” phase of the Wetzel et al. (2013) scenario the galaxies are completely unaffected by environment. A more recent

Table 1. Measured and derived quantities for 19 XMM2215 cluster galaxies at $z \sim 1.46$ with KMOS H-band observations. The complete version of this table (now only three objects) for the full sample of 19 galaxies will be available after the paper is published in A&A.

Id	spect. z	$\log[\text{NII}]/\text{H}\alpha$	$\log(M/M_{\odot})$	O/H (PP04)	R/R_{200}
29284	1.461	-0.57 ± 0.08	10.36	8.57 ± 0.05	0.74
29609	1.459	[NII] on OH	10.49	*	0.44
30183	1.458	[NII] on OH	10.18	*	0.27

study of Roberts et al. (2019) used X-ray data for $z < 0.1$ clusters to study the influence of the ICM on the quenching of satellite galaxies. They found that the quenched fraction of galaxies increases modestly at ICM densities below a threshold before increasing sharply beyond this threshold toward the cluster center. They found their results to be consistent with a picture where cluster galaxies experience an initial, slow-quenching mode driven by steady gas depletion, followed by rapid quenching associated with ram pressure of cold-gas stripping near the cluster center, in agreement with the *slow-then-rapid* quenching scenario of Maier et al. (2019).

These investigations of lower redshift clusters demonstrated that the density of the ICM is an important parameter influencing the quenching of galaxies and that enhanced metallicities in massive clusters are a valuable quenching tracer. To extend these studies to $z > 1$ we aim to study clusters of galaxies found as overdensities of galaxies which are unambiguously identified through their hot diffuse medium, manifested through X-ray emission. One of the most massive galaxy clusters at $z > 1.5$ is XMMXCS J2215.9-1738 (hereafter XMM2215) at $z \sim 1.46$ with extended X-ray emission from the hot gas, found from XMM Newton X-ray data as part of the XMM Cluster Survey (Stanford et al. 2006). Given its high mass and high ICM density possibly favouring stronger RPS, this is one of the best cluster targets to study environmental effects on metallicities and quenching at $z > 1$, because more pronounced environmental effects than in other less massive clusters at $z > 1$ are expected.

A pioneering study of the MZR in XMM2215 was done by Hayashi et al. (2011). They claimed to find a similar MZR relation for cluster and field galaxies at $z \sim 1.5$. However, a caveat of their study was the use of quite low-resolution ($R \sim 700$) Subaru-MOIRCS spectroscopy which made night-sky lines correction difficult, and therefore night-sky lines contamination of [NII] influencing metallicities measurements (as mentioned above) could not be always avoided. For most of their observed galaxies the signal-to-noise (S/N) of the [NII] fluxes was quite low ($S/N < 2 - 3$) or only upper limits for [NII] line fluxes could be measured. The new KMOS observations which we present in this study contain also some of the galaxies studied by Hayashi et al. (2011). The much better resolution of KMOS ($R \sim 4000$ in H-band vs. $R \sim 700$ with MOIRCS) and better S/N from the higher sensitivity IFU data enables us to improve the S/N of H α and [NII] in all galaxies in common with Hayashi et al. (2011). Additionally, we revise the study of the chemical enrichment in XMM2215 by Hayashi et al. (2011) now additionally using the information from the phase-space diagram about the position of galaxies in the cluster, by separating galaxies from the infalling and virialized regions.

The paper is structured as follows: In Sect. 2 we present the selection of the XMM2215 cluster EL galaxies at $z \sim 1.5$, their KMOS spectroscopy and data reduction. We describe the EL flux measurements and present the derivation of SFRs, metallicities, and stellar masses of the observed cluster galaxies. In Sect. 3 we present the phase-space diagram, the mass – specific SFR (SSFR) relation and the MZR at $z \sim 1.5$. We investigate

how the cluster environment affects the chemical enrichment. In Sect. 4, using the position of galaxies in the BPT (Baldwin et al. 1981) diagram, we discuss the difference in metallicities calibrations and resulting different metallicities enhancements of cluster objects compared to field galaxies. We then discuss the slow quenching scenario in a massive cluster at $z > 1$ implied by our findings and the comparison with literature metallicities studies in clusters at $z > 1$. Finally, we summarize our conclusions. A concordance cosmology with $H_0 = 70 \text{ km s}^{-1} \text{ Mpc}^{-1}$, $\Omega_0 = 0.25$, $\Omega_{\Lambda} = 0.75$ is used throughout this paper. We assume a Salpeter (Salpeter 1955) initial mass function (IMF) for all derived stellar masses and SFRs and correct existing measurements used in this paper to a Salpeter IMF. We note that metallicity and abundance are taken to denote oxygen abundance, O/H, throughout this paper, unless otherwise specified. In addition, we use dex throughout to denote the antilogarithm, i.e., 0.3 dex is a factor of two.

2. Data and measurements

2.1. KMOS observations and data reduction of cluster SF galaxies in XMM2215

XMM2215 was discovered in the XMM Cluster Survey (Stanford et al. 2006). It is a massive $z \sim 1.46$ cluster with an older estimation of the mass of $M_{200} \sim 2.1 \cdot 10^{14} M_{\odot}$ (Hilton et al. 2010; Stott et al. 2010), and a newer estimation in this study of a higher mass of $M_{200} \sim 6.3 \cdot 10^{14} M_{\odot}$ (see Sect. 3.1). One advantage for observational environmental studies in this cluster compared to other clusters at $z > 1$ is its wealth of spectroscopic redshifts published not only for star forming but also for passive galaxies (Hilton et al. 2009, 2010; Hayashi et al. 2011; Beifiori et al. 2017; Chan et al. 2018). This enables to characterize the accretion state of cluster member galaxies by identifying virialized and infalling regions (see Sect. 3.1).

The targets for the KMOS H-band observations were selected from the list of $1.44 < z < 1.48$ [OII] emitters, with a flux larger than $2 \times 10^{-17} \text{ ergs/s/cm}^2$, identified from narrowbands NB912 and/or NB921 by Hayashi et al. (2014). Most of the targets have been already spectroscopically confirmed before the KMOS observations. VLT/KMOS H-band observations were carried out in 2016 in the night October 19th/20th with a nod-to-sky strategy and each observing block (OB) consisting of several ABA ABA sequences, where “A” denotes that the IFUs were placed on the science targets, and “B” indicates that the IFUs were observing blank sky. The integration time of each exposure was 300 s with a total exposure time of 9900 s. Seeing conditions measured in the optical by the DIMM seeing monitor ranged between 0.6 and 1.0 arcsec.

The KMOS data reduction was carried out with the official ESO-KMOS pipeline version 1.4.3 with the default settings of the pipeline except the default of the pipeline to first combine exposures from a single OB before then combining these OBs into final data cubes. Since the best data quality in the co-addition of individual exposures is achieved using sigma clipping, we mod-

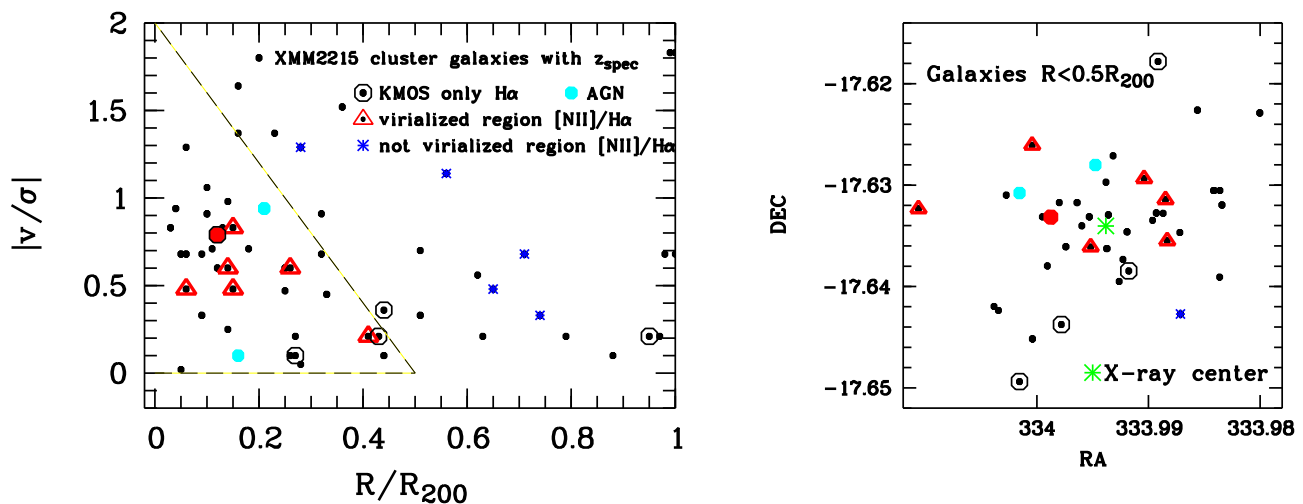


Fig. 2. Left: Phase-space diagram showing 58 XMM2215 cluster galaxies with spectroscopic redshifts inside R_{200} . The galaxies with KMOS H-band observations are shown by larger symbols, as indicated in the legend. The dashed large triangle in the lower left-hand corner shows the virialized region, as derived by Rhee et al. (2017) using cosmological hydrodynamic simulations of groups and clusters. Right: Spatial distribution of 42 galaxies in the central part of the XMM2215 cluster at $R < 0.5R_{200}$ (symbols like in the left panel). The red filled circle indicates one galaxy with measured $[\text{NII}]/\text{H}\alpha$ with much higher mass than the galaxies shown as red triangles. A green star symbol shows the cluster center determined with extended X-ray emission (Stanford et al. 2006).

ified the default approach and ran the sigma clipping and cube combination on all individual 33 exposures (from four OBs) at once.

2.2. KMOS ELs measurements

To measure the main ELs $\text{H}\alpha$ and $[\text{NII}]\lambda 6584$ from the KMOS H-band observations, we use the IDL publicly available software KUBEVIZ (Fossati et al. 2016) applied on each extracted 1D spectrum. To measure the ratio of the $\text{H}\alpha$ and the (typically) fainter $[\text{NII}]\lambda 6584$ EL flux to compute O/H metallicities, we extracted 1D spectra summed over 25 spaxels centered on the $\text{H}\alpha$ EL of the respective KMOS data cube, corresponding to an aperture of about 1 square arcsecond. This typically corresponds to the area where KUBEVIZ measures $S/N > 3$ per spaxel in $[\text{NII}]\lambda 6584$. For the total $\text{H}\alpha$ fluxes used to compute SFRs we extracted 1D spectra over slightly larger areas, including all spaxels where KUBEVIZ measures $S/N > 3$ in $\text{H}\alpha$. Starting from an initial redshift, KUBEVIZ is fitting simultaneously the “lineset” $\text{H}\alpha$ and $[\text{NII}]\lambda 6584$. This “lineset” is described by a combination of 1D Gaussian functions keeping the velocity separation of the lines fixed according to the line wavelengths (see Fig. 1). The continuum level is evaluated inside two symmetric windows around each lineset. During the fit, KUBEVIZ takes into account the noise from the noise data cube, thus optimally suppressing sky line residuals.

From the 20 observed XMM2215 targets we could detect the $\text{H}\alpha$ EL for 19 galaxies (see Table 1). The $[\text{NII}]\lambda 6584$ EL could be detected in twelve galaxies, while in the remaining seven galaxies $[\text{NII}]\lambda 6584$ was either affected by a strong OH line or too faint to be detected, yielding only an upper limit in two cases. For one galaxy among the seven, the $\text{H}\alpha$ line was detected, but heavily affected by a strong night-sky line, so no reliable measurement of the $\text{H}\alpha$ EL flux was possible. Two of the twelve galaxies with detected $[\text{NII}]\lambda 6584$ turn out to be AGNs because they have an $[\text{NII}]\lambda 6584$ flux comparable with the $\text{H}\alpha$ flux (see Table 1). The remaining ten galaxies with detected $[\text{NII}]\lambda 6584$ include seven galaxies in the inner region of the cluster ($R < 0.5R_{200}$)

and three galaxies outside. Note that two additional galaxies with upper limits on $[\text{NII}]\lambda 6584$, see Table 1, are also shown in Fig. 2 with blue symbols.

2.3. Stellar masses, SFRs, oxygen abundances

Stellar masses of the XMM2215 cluster galaxies were calculated using the code *Lephare* of Arnouts & Ilbert (2011), which fits stellar population synthesis models (Bruzual & Charlot 2003) to the available SUBARU B, R_c , i' , z' and WFCAM/UKIRT K-band photometry described in Hayashi et al. (2014). This code is a simple χ^2 minimization algorithm that finds the best match of templates for the given data. We do not fit templates with stellar ages of less than 0.5 Gyr and larger than 5 Gyr. This is a valid assumption since at $z \sim 1.5$ the Universe is only ~ 4.5 Gyr old. In addition, we kept the redshift fixed and also limited the number of extinction $E_{(B-V)}$ values (0 to 0.5, in 0.1 steps). We are confident in the robustness of the calculated masses since the $z - K$ color encompasses the redshifted 4000\AA break and thus is sensitive to galaxy mass-to-light ratios (Kauffmann et al. 2003).

It turns out that one galaxy (39683, red filled circle in Fig. 2) of our sample of ten SF galaxies with detected $[\text{NII}]\lambda 6584$ has higher mass, $\log(M/M_\odot) \sim 11.4$. For our study of environmental effects on metallicities we restrict our cluster sample to nine galaxies with $[\text{NII}]/\text{H}\alpha$ measured and $\log(M/M_\odot) < 11$, including six objects at $R < 0.5R_{200}$ (our *SFvirialized* sample). One reason for the exclusion is that this high mass galaxy could have a higher metallicity also due to its higher mass and not to environmental effects. Additionally, a narrower range in stellar masses allows to better disentangle mass and environmental effects on metallicities.

Since we do not have measurements of $\text{H}\beta$ we cannot use an observed Balmer decrement to derive extinction. Therefore, the $\text{H}\alpha$ line luminosities $L(\text{H}\alpha)$ were corrected for three values of assumed extinction $A_V = 0, 0.5, 1$ and then transformed into SFRs by applying the Kennicutt (1998) conversion: $\text{SFR}(M_\odot\text{yr}^{-1}) = 7.9 \times 10^{-42} L(\text{H}\alpha)\text{ergs/s}$.

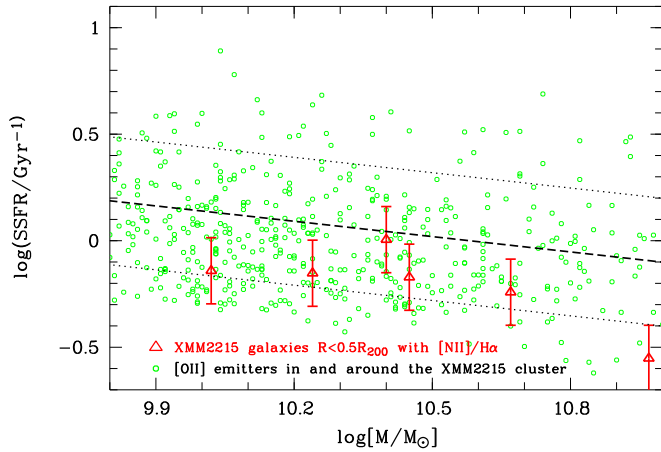


Fig. 3. Mass–SSFR relation for the [OII] emitters in and around the XMM2215 cluster (green open circles) and the six XMM2215 cluster galaxies of the *SFvirialized* sample (red triangles). The oblique solid line shows the MS at $z \sim 1.46$ and its dispersion (indicated by the dotted lines) using Eq. 1 in Peng et al. (2010).

To estimate the chemical abundances, a number of diagnostics have been developed based on strong ELs, [O II] $\lambda 3727$, H β , [O III] $\lambda 5007$, H α and [N II] $\lambda 6584$. At higher redshifts, these ELs move to the near-infrared, and studies of metallicities up to $z \sim 2.5$ use mostly the N2-calibration or the O3N2-calibration of Pettini & Pagel (2004) to derive oxygen abundances. For easier comparison with existing publications of the MZR at $z > 1$ we therefore use the N2 and O3N2 metallicity calibrations for this study. We derive oxygen abundances from [NII]/H α using the N2-method of Pettini & Pagel (2004). One galaxy from our *SFvirialized* sample has an [OIII]/H β measurement (with large error bars) and another galaxy has an upper limit for [OIII]/H β , both from the work of Hayashi et al. (2011), indicating a ratio of [OIII]/H β smaller than one. In order to exploit the O3N2 metallicity calibration, we therefore assume a range of [OIII]/H β between 0.5 and 1 for the six galaxies of the *SFvirialized* sample and compute their metallicities also using the O3N2-method of Pettini & Pagel (2004).

3. Results

3.1. Spatial distribution and phase-space diagram

A phase-space diagram is a useful tool to characterize the accretion state of cluster member galaxies relatively free from effects due to the 2D projected positions with respect to the cluster center (see Fig. 2, comparing left to right panel). To investigate cluster membership for XMM2215 we collected the redshift information from literature (Hilton et al. 2009, 2010; Hayashi et al. 2011; Beifiori et al. 2017; Chan et al. 2018) yielding a sample of 108 galaxies with published spectroscopic redshifts. We then used the 3σ -clipping technique of Yahil & Vidal (1977), which assumes that clusters are relaxed isothermal spheres and the velocity distribution of cluster galaxies follows an underlying Gaussian distribution. 74 galaxies out of the 108 lie inside 3σ .

A mass model of the cluster was computed assuming that the cluster is a singular isothermal sphere. R_{200} is the radius that encloses a mean density 200 times the critical density at a given redshift (roughly equivalent to the virial radius of Carlberg et al. 1997) and is calculated as $\sqrt{3}/10 \cdot \sigma_z/H(z)$, where σ_z is the velocity dispersion of the cluster and $H(z)$ the redshift dependent

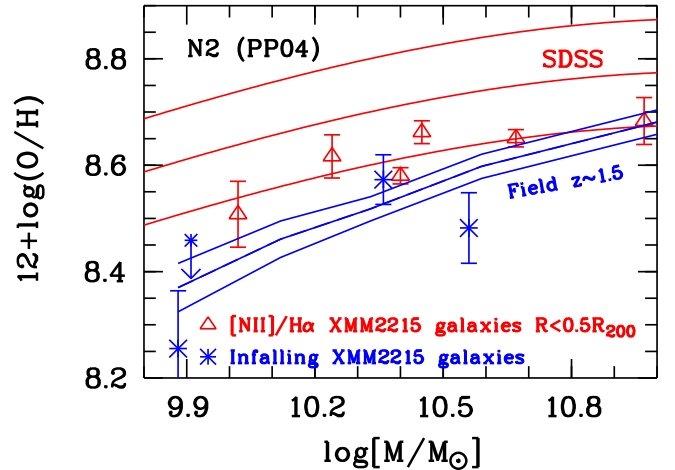


Fig. 4. MZR for cluster and field galaxies at $z \sim 1.5$, using the N2-method of Pettini & Pagel (2004) to derive oxygen abundances. The SDSS local MZR relation is shown by the red solid lines using the fit given by Kewley & Ellison (2008) for the N2 calibration. The blue solid lines show the mean location of field galaxies at $z \sim 1.5$ from Kashino et al. (2017). Red triangles are XMM2215 cluster galaxies from the *SFvirialized* sample, while blue star symbols are XMM2215 infalling galaxies (see phase-space diagram, Fig. 2).

Hubble parameter. From this iterative method based on the technique of Carlberg et al. (1997) we obtained $R_{200} \sim 1.23 Mpc$ and $\log(M_{200}/M_\odot) \sim 14.8$. These values are slightly higher than those derived by Hilton et al. (2010) using a similar analysis, but it should be noted that Hilton et al. (2010) used only 44 spectroscopic redshifts (compared to 74 used by us), and we also used spectroscopic redshifts of passive galaxies more recently published by Beifiori et al. (2017) and Chan et al. (2018).

From the 74 objects with spectroscopic redshifts inside 3σ we found 58 galaxies to lie inside R_{200} , as depicted in Fig. 2. The red triangle symbols represent our main *SFvirialized* sample of cluster galaxies with [NII]/H α measured and lying in the virialized region of the cluster, as indicated by the large triangle in the lower left-hand corner derived by Rhee et al. (2017) using cosmological hydrodynamic simulations of groups and clusters.

3.2. *SF* XMM2215 cluster galaxies with enhanced metallicities

Fig. 3 shows the mass-SSFR relation of star-forming galaxies in and around the XMM2215 cluster. Peng et al. (2010) derived a formula of the evolution of the SSFR as a function of mass and time that we use to calculate the mean SSFR as a function of stellar mass at $z \sim 1.5$ (main sequence, MS). For this, we assume a dependence of the SSFR on mass as observed for local SDSS galaxies, an increase in the mean SSFR from $z \sim 0$ to $z \sim 1.5$ as derived by Peng et al. (2010), and a dispersion (indicated by the dotted oblique lines) of a factor of 0.3 dex about the mean relation. SFRs for [OII] emitters, identified from narrowbands NB912 and/or NB921 by Hayashi et al. (2014), are derived from their [OII] fluxes using the relation recommended by Maier et al. (2015). For the six galaxies in the *SFvirialized* sample we assumed three values of extinction, $A_V = 0, 0.5$, and 1, and then transformed their H α fluxes into SFRs by applying the Kennicutt (1998) conversion. The error bars of the six triangles

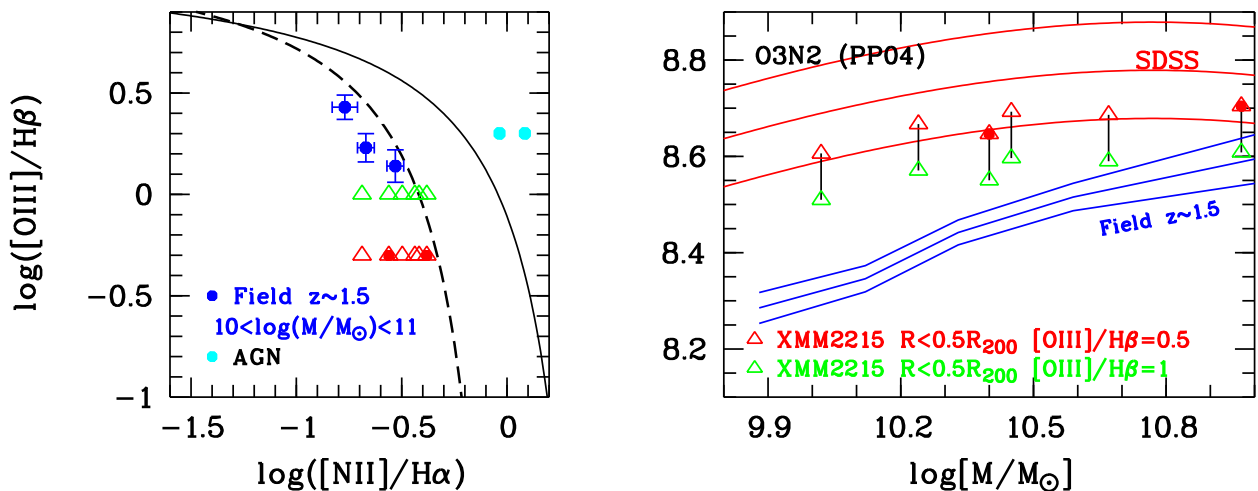


Fig. 5. Left: Diagnostic diagram BPT (Baldwin et al. 1981) to distinguish star formation-dominated galaxies from AGNs. The theoretical (solid) curve of Kewley et al. (2001) and the empirical (dashed) curve of Kauffmann et al. (2003b) separate star-forming galaxies (below/left of the curves) from AGNs (above/right of the curves). Blue symbols with error bars show the EL ratios from co-added spectra of $z \sim 1.5$ field galaxies of Kashino et al. (2017) for three mass bins. Red and green triangles indicate possible low $[\text{OIII}]/\text{H}\beta$ values for the *SFvirialized* sample with measured $[\text{NII}]/\text{H}\alpha$, motivated by the $[\text{OIII}]/\text{H}\beta$ less than one ratio measurements of Hayashi et al. (2011) for two galaxies (filled red triangles). Right: MZR for cluster and field galaxies at $z \sim 1.5$ using the O3N2-method of Pettini & Pagel (2004) to derive oxygen abundances. The SDSS local MZR relation is shown by the red solid lines for the O3N2 O/H calibration using the fit given by Kewley & Ellison (2008). The blue solid lines show the mean location of field galaxies at $z \sim 1.5$ of Kashino et al. (2017). Red triangles are XMM2215 cluster galaxies from the *SFvirialized* sample (see phase-space diagram, Fig. 2); the two red filled triangles indicate the two galaxies with low $[\text{OIII}]/\text{H}\beta$ of Hayashi et al. (2011).

in Fig. 3 indicate the range of SFRs for A_V values between 0 and 1.

Five out of the six *SFvirialized* galaxies lie in the lower SSFR part of the MS region, while the most massive one lies just below the MS region assuming a maximum of $A_V = 1$, but it would lie in the lower SSFR part of the MS region for a plausible higher extinction value at higher masses of $A_V > 1$. Therefore, we conclude that the six *SFvirialized* galaxies are still star-forming, although with slightly lower SSFRs, lying in the lower SSFR part of the MS region. We note that their slightly lower SFRs and higher metallicities (as discussed below) are quite in agreement with expectations of the link between SFRs and O/Hs described by the fundamental metallicity relation (e.g., Mannucci et al. 2010).

Fig. 4 and the right panel of Fig. 5 show the MZR of the six *SFvirialized* cluster galaxies (triangles) compared to the infalling galaxies (blue asterisks), Kashino et al. (2017) field galaxies at $z \sim 1.5$ from the FMOS-COSMOS survey (blue solid lines) and the local SDSS MZR (red solid lines). All metallicities were computed with the same method, either N2 or O3N2. The cluster galaxies in the virialized region of the XMM2215 cluster (red triangles) show in general higher metallicities compared to infalling galaxies and field galaxies at $z \sim 1.5$. The typical O/H enhancement of *SFvirialized* cluster galaxies is ~ 0.1 dex using the N2 calibration and larger, ~ 0.2 dex, using the O3N2 calibration, with cluster galaxies reaching metallicities similar to SDSS values at the respective mass. As described in Sect. 2.3, motivated by the $[\text{OIII}]/\text{H}\beta$ less than one flux ratio measurements for two out of six galaxies in the *SFvirialized* sample (Hayashi et al. 2011), the depicted O/Hs in Fig. 5 assume an $[\text{OIII}]/\text{H}\beta$ flux ratio between 0.5 and 1. For an $[\text{OIII}]/\text{H}\beta$ flux ratio larger than one value, the O/Hs of the remaining four *SFvirialized* objects could be slightly lower than the values indicated by the green triangles in the MZR diagram, but the effect of enhanced O3N2 metallicities for cluster galaxies would still remain, at least at the lower

masses. In Sect. 4 we discuss the quenching scenario implied by the enhanced metallicities of XMM2215 cluster galaxies.

4. Discussion and Summary

4.1. Enhancement of metallicities in cluster galaxies using N2 vs. O3N2 metallicities

Our study of metallicities of XMM2215 cluster galaxies shows a typical enhancement of metallicities of cluster galaxies inside $0.5R_{200}$ by ~ 0.1 dex when using the N2-calibration (Fig. 4) compared to ~ 0.2 dex when using the O3N2-calibration (Fig. 5), with cluster galaxies reaching metallicities similar to SDSS values at the respective mass. A higher difference between local SDSS metallicities and O/Hs of $z > 1$ field galaxies using O3N2 compared to the N2 calibration was already noted by Steidel et al. (2014), see their Figs. 23 and 24, and by Salim et al. (2015), their Fig. 1, when comparing O/Hs of $z > 2$ field galaxies with SDSS. As one of the reasons for this effect, Salim et al. (2015) mentioned that the linear N2 calibration is too crude to capture the saturation of N2 at high metallicities.

To further explore the different metallicity enhancement dependent on O/H calibration, we show in the left panel of Fig. 5 the position of *SFvirialized* objects and COSMOS field galaxies at $z \sim 1.5$ in the diagnostic diagram BPT (Baldwin et al. 1981). The two objects identified as AGNs by their $[\text{NII}]/\text{H}\alpha$ flux comparable to $\text{H}\alpha$ flux are shown by the solid filled cyan circles at a typical, expected for AGNs, flux ratio of the ELs $[\text{OIII}]/\text{H}\beta$ of two. The reason for the larger offset in the enhancement of metallicities of cluster galaxies compared to field in the MZR diagram using O3N2 vs. N2 is revealed by the different positions of field galaxies and cluster galaxies in a diagram using *two* line ratios $[\text{OIII}]/\text{H}\beta$ and $[\text{NII}]/\text{H}\alpha$. The N2-calibration uses less information, only *one* ratio $[\text{NII}]/\text{H}\alpha$, and cannot capture at higher metallicities the decrease of $[\text{OIII}]/\text{H}\beta$ while the $[\text{NII}]/\text{H}\alpha$ ratio remains rather constant. Although we observe an enhancement in

metallicities of $z \sim 1.5$ cluster galaxies compared to field also using the $[\text{NII}]/\text{H}\alpha$ ratio (Fig. 4), the additional information on the $[\text{OIII}]/\text{H}\beta$ ratio makes this metallicity enhancement more significant (Fig. 5).

Quai et al. (2018) claimed that galaxies with lower $[\text{OIII}]\lambda 5007/\text{H}\beta$, like at least two of the cluster galaxies in our *SFvirialized* sample, are good candidates for galaxies in the act of quenching star formation. They argued that, after a few Myr after the onset of quenching of star formation, the shortest-lived (i.e., most massive) O stars and their hard UV photons rapidly disappear, and this causes a fast decrease of the luminosity of high-ionization lines (e.g., $[\text{OIII}]$). However, Balmer lines (ELs with lower ionization) should be still observable because their luminosity decreases more slowly due to photo-ionization from lower mass (longer lived) OB stars. Therefore, galaxies in the process of quenching star formation should be selectable based on their low $[\text{OIII}]\lambda 5007/\text{H}\beta$ ratios.

Depending on the O/H calibration used (N2 or O3N2) and given the information on low $[\text{OIII}]/\text{H}\beta$ ratios available only for two out of six galaxies, Figs. 4 and 5 indicate either an enhancement of metallicities of cluster galaxies compared to field only at lower masses ($\log(M/M_\odot) < 10.5$) or at all masses studied ($10 < \log(M/M_\odot) < 11$). The first scenario, an enhancement of O/H of cluster galaxies with $\log(M/M_\odot) < 10.5$ is quite in agreement with the findings of Kulas et al. (2013) in a protocluster at $z > 2$, while the second, an enhancement of O/H of cluster galaxies with $10 < \log(M/M_\odot) < 11$ is rather in agreement with the results of Shimakawa et al. (2015) in a protocluster at $z > 2$. We note, however, that the results of Kulas et al. (2013) and Shimakawa et al. (2015) were based on stacking (also of galaxies with not detected $[\text{NII}]$ ELs), while our results are based on *individual* measurements of $[\text{NII}]/\text{H}\alpha$. The studies of Kacprzak et al. (2015) and Tran et al. (2015) for cluster galaxies at $z > 1.6$ used the N2-calibration from stacking and found a similar MZR for cluster and field galaxies. Based on the findings of Fig. 5 as discussed above, it is possible that additional information on $[\text{OIII}]$ and $\text{H}\beta$ and the use of O3N2 could reveal a slight difference in the MZR of cluster and field galaxies also for the $z > 1.6$ clusters studied by Kacprzak et al. (2015) and Tran et al. (2015).

4.2. Slow-quenching implied by enhanced metallicities of cluster galaxies at $z \sim 1.5$

The enhanced metallicities of $z \sim 1.5$ cluster galaxies inside $0.5R_{200}$ compared to $z \sim 1.5$ field galaxies can be interpreted as a quenching indicator, based on the comparison of observed quantities with metallicity-SFR-mass bathtub model predictions with inflowing gas (Lilly et al. 2013) done in lower redshift clusters by Maier et al. (2016, 2019). The interpretation is that the gas metallicities are increasing because their ISM is no longer diluted by the inflow of pristine gas, after the hot halo gas reservoir was stripped in the cluster environment, likely around $0.5R_{200}$, initiating strangulation.

An enhancement of O/Hs of $z \sim 1.5$ cluster galaxies with $10 < \log(M/M_\odot) < 11$ compared to field galaxies is also in agreement with the results of Shimakawa et al. (2015), who measured metallicities based on $[\text{NII}]/\text{H}\alpha$ from stacked spectra in protoclusters at $z > 2$. Shimakawa et al. (2015) also discussed one strangulation scenario based on their result: for infalling cluster galaxies, once an infalling galaxy is incorporated into a common cluster halo, the gas reservoir of the galaxy may be stripped or truncated due to the interactions with the cluster environment. This can not only expel low metallicity gas trapped in

the outer region of the galaxy, but also terminate the fresh pristine gas accretion on to the galaxy, increasing the retained gas metallicity.

The current KMOS study of cluster galaxies in XMM2215 shows, using *individual* metallicity measurements, that environmental effects on metallicities implying quenching are starting to act already at $z > 1$. Maier et al. (2019) discussed how the hot gas reservoir and the cold gas in the disk may be influenced for infalling galaxies into clusters, depending on the strength of the cluster potential and the ICM density. Gas can be removed from infalling galaxies if the ram pressure exceeds the restoring force per unit area (gravitational restoring pressure) exerted by the galaxy, as first derived by Gunn & Gott (1972). XMM2215 contains only a few passive galaxies known and with spectroscopic redshifts determined (Beifiori et al. 2017; Chan et al. 2018). Therefore, it is plausible that the ICM density in this cluster implies a ram pressure higher than the restoring pressure of the *hot* halo gas reservoir of cluster galaxies, but not higher than the restoring pressure of the *cold* gas in the disk out of which stars are currently born.

Compared to the slow-then-rapid quenching scenario discussed by Maier et al. (2019) and Roberts et al. (2019) we think that we see only the “slow” quenching in XMM2215 SF cluster galaxies at $z \sim 1.5$ traced by enhanced metallicities. As discussed in Maier et al. (2019) based on comparisons with high-resolution cosmological hydrodynamic simulations of Bahé et al. (2013), the ram pressure is probably only slightly larger than $3 \times 10^{-14} \text{ N/m}^2$ in XMM2215, larger than the restoring pressure of hot gas and enough to strip the more extended, less dense and less tightly bound hot gas. This slow quenching is also quite in agreement with results of Hayashi et al. (2017, 2018) who used ALMA to measure CO(2-1) ELs and dust continuum and derived molecular gas masses for several XMM2215 cluster galaxies. They discussed that the main component of the stripped gas is the neutral gas reservoir, while the molecular gas (observed with ALMA) is relatively much less affected by the ram-pressure, so the galaxies continue to form stars from the molecular gas, in agreement with our slow quenching scenario. The ICM density in XMM2215 probably did not yet reach the threshold found by Roberts et al. (2019) to initiate the “rapid” quenching, a ram pressure threshold required to strip the cold gas of cluster galaxies, cold gas which is denser and sits much closer to the galactic center.

4.3. Summary

To study environmental effects on the chemical enrichment and quenching of cluster galaxies, we used KMOS spectroscopy of $\text{H}\alpha$ and $[\text{NII}]\lambda 6584$ in the massive cluster XMM2215 at $z \sim 1.5$ to measure oxygen abundances and estimate SFRs. Using the phase-space diagram results of Fig. 2 we identified XMM2215 SF cluster galaxies in a virialized region with $R < 0.5R_{200}$ and smaller line-of-sight velocities. Studying the metallicities of a sub-sample of the cluster galaxies with KMOS H-band observations and located in the virialized region (*SFvirialized* sample), we found evidence for enhanced metallicities by 0.1–0.2 dex for these galaxies compared to infalling and field galaxies at similar redshifts (Figs. 4 and 5). These cluster galaxies are still star-forming, although with slightly lower SFRs (see Fig. 3).

These findings indicate a strangulation scenario in which the ICM density toward the cluster center becomes high enough such that RPS can remove the hot halo gas reservoir of cluster galaxies enhancing metallicities and initiating slow quenching, while the galaxies continue to form stars using cold gas in the

disk and enhance their metallicities because no fresh pristine gas accretion dilutes their ISM. Additional spectroscopic observations not only of [NII] and $H\alpha$, but also of [OIII] and $H\beta$ for a larger sample of cluster galaxies at $z > 1$ are needed to put these interesting tentative results based on a small sample on solid footings.

References

- Arnouts, S., & Ilbert, O., 2011, *Astrophysics Source Code Library*, ascl:1108.009
- Bahé, Y. M., McCarthy, I. G., Balogh, M. L., & Font, A. S., 2013, *MNRAS*, 430, 3017
- Baldwin, J. A., Phillips, M. M., & Terlevich, R., *PASP*, 93, 5
- Beifiori, A., Mendel, J. T., Chan, J. C. C., et al. 2017, *ApJ*, 846, 120
- Bruzual & Charlot, 2003, *MNRAS*, 344, 1000
- Carlberg, R. G., Yee, H. K. C., & Ellingson, E., 1997, *ApJ*, 478, 462
- Chan, J. C. C., Beifiori, A., Saglia, R. P. et al. 2018, *ApJ*, 856, 8
- Chiang, Y.-K., Overzier, R. A., Gebhardt, K., & Henriques, B., *ApJ*, 844, 23
- Dickinson, M., Papovich, C., Ferguson, H. C., et al., 2003, *ApJ*, 587, 25
- Drory, N., Salvato, M., Gabasch, A., et al., 2005, *ApJ*, 619, 131
- Fossati, M., Fumagalli, M., Boselli, et al., 2016, *MNRAS*, 455, 2028
- Gunn J. E., Gott J. R. I., 1972, *ApJ*, 176, 1
- Hayashi, M., Kodama, T., Koyama, Y., et al., 2011, *MNRAS*, 415, 2670
- Hayashi, M., Kodama, T., Koyama, Y., et al., 2014, *MNRAS*, 439, 2571
- Hayashi, M., Kodama, T., Kohno, K., et al., 2017, *ApJ*, 841, L21
- Hayashi, M., Tadaki, K.-i., Kodama, T., et al., 2018, *ApJ*, 856, 118
- Hilton, M., Stanford, S. A., Stott, J. P., et al. 2009, *ApJ*, 697, 436
- Hilton, M., Lloyd-Davies, E., Stanford, S. A., et al. 2010, *ApJ*, 718, 133
- Kauffmann, G., Heckman, T. M., White, S. D. M., et al., 2003, *MNRAS*, 341, 33
- Kauffmann, G., Heckman, T. M., Tremonti, C. et al., 2003b, *MNRAS*, 346, 1055
- Kacprzak, G. G., Yuan, T., Nanayakkara, T., et al., 2015, *ApJ*, 802, 26
- Kashino, D., Silverman, J. D., Sanders, D., et al., 2017, *ApJ*, 835, 88
- Kennicutt, R. C., Jr. 1998, *ARA&A*, 36, 189
- Kewley, L. J., Heisler, C. A., Dopita, M. A., & Lumsden, S., 2001, *ApJS*, 132, 37
- Kewley, L.J. & Dopita, M.A. 2002 *ApJSS*, 142, 35
- Kewley, L. J., & Ellison, S. L., 2008, *ApJ*, 681, 1183
- Kulas, K. R., McLean, I. S., Shapley, A. E., et al., 2013, *ApJ*, 774, 130
- Lilly, S. J., Carollo, C. M., Pipino, A. et al., 2013, *ApJ*, 772, 119
- Maier, C., Ziegler, B. L., Lilly, S. J., et al., 2015, *A&A*, 577, 14
- Maier, C., Kuchner, U., Ziegler, B. L., et al., 2016, *A&A*, 590, A108
- Maier, C., Ziegler, B. L., Haines, C. P., & Smith, G. P., 2019, *A&A*, 621, A131
- Magdis, G. E., Bureau, M., Stott, J. P., et al., 2016, *MNRAS*, 456, 4533
- Mannucci, F., Cresci, G., Maiolino, R. et al. 2010, *MNRAS*, 408, 2115
- Pettini & Pagel 2004, *MNRAS*, 348, 59
- Peng, Y.-j., Lilly, S. J., Kovač, K., et al., 2010, *ApJ*, 721, 193
- Quai, S., Pozzetti, L., Citro, A., Moresco, M., & Cimatti, A., 2018, *MNRAS*, 478, 3335
- Rhee, J., Smith, R., Choi, H., et al., 2017, *ApJ*, 843, 128
- Roberts, I. D., Parker, L. C., Brown, T., et al., 2019, *arXiv:1902.02820*
- Salim, S., Lee, J. C., Dave, R., & Dickinson, M., 2015, *ApJ*, 808, 25
- Salpeter, E. E., 1955, *ApJ*, 121, 161
- Shimakawa, R., Kodama, T., Tadaki, K.-i., et al., 2015, *MNRAS* 448, 666
- Springel, V. 2010, *MNRAS*, 401, 791
- Stanford, S. A., Romer, A. K., Sabirli, K., et al. 2006, *ApJL*, 646, L13
- Steidel, C. C., Rudie, G. C., Strom, A. L., et al., 2014, *ApJ*, 795, 165
- Steinhauser, D., Schindler, S., & Springel, V., 2016, *A & A*, 591, A51
- Stott, J. P., Collins, C. A., Sahlén, M., et al. 2010, *ApJ*, 718, 23
- Tran, K.-V. H., Nanayakkara, T., Yuan, T., Kacprzak, G. G., et al., 2015, *ApJ*, 811, 28
- Valentino, F., Daddi, E., Strazzullo, V., et al., 2015, *ApJ*, 801, 132
- Wetzel, A. R., Tinker, J. L., Conroy, C., & van den Bosch, F. C., 2013, *MNRAS*, 432, 336
- Yahil, A., & Vidal, N. V., 1977, *ApJ*, 214, 347
- Zahid, H. J., Kashino, D., Silverman, J. D., et al., 2014, *ApJ*, 792, 75
- Kewley, L. J., Daddi, E.,